Identification of pyroptosis-related genes in neuropathic pain based on bioinformatics analysis

XIN LI*, DI ZHANG*, HUIMEI SHI, BEI JING, ZHENNI CHEN, YACHUN ZHENG, SHIQUAN CHANG, LI GAO and GUOPING ZHAO

College of Traditional Chinese Medicine, Jinan University, Guangzhou, Guangdong 510632, P.R. China

Received June 2, 2022; Accepted October 28, 2022

DOI: 10.3892/etm.2022.11745

Abstract. Pyroptosis is defined as inflammation-induced programmed cell death. However, gene expression levels related to pyroptosis and their role in neuropathic pain (NP) remain unclear. The present study aimed to develop and validate an NP-predictive signature based on the genes associated with pyroptosis. Gene expression level profiles were downloaded from the Gene Expression Omnibus database. Weighted gene co-expression network analysis was used to identify the pyroptotic genes most highly associated with NP. NP-related pyroptosis gene signature was constructed using multivariate logistic regression. A rat model of neuropathic pain was established through chronic constriction injury to analyse the inflammatory infiltration and myelin damage around the sciatic nerve, and examine the expression levels of macrophage markers S100 calcium-binding protein β (S100β) and ionized calcium-binding adapter molecule 1 (Iba-1). Finally, flow cytometry analysis was used to examine the lipopolysaccharide (LPS)-induced cell death ratio of RSC96 cells (Schwann cells), while the expression levels of LPS-induced pyroptosis-related genes in RSC96 cells were measured via reverse transcription-quantitative PCR. The results demonstrated that pyroptosis-related genes (gasdermin D, NLR family pyrin domain containing 3, neuronal apoptosis inhibitory protein and NLR family CARD domain containing 4) were identified to increase the risk of NP. NP-related pyroptosis signatures were constructed based on these four genes. Moreover, the high-risk group had a higher level of macrophage infiltration compared with the low-risk group, as determined by the CIBERSORT algorithm. H&E staining results showed that the myelin structure of the sciatic nerve tissue of chronic constriction injury (CCI) rats was destroyed and inflammatory cells infiltrated around neurons. The results of immunohistochemistry showed that compared with in the sham group, the expression levels of Iba-1 and sS100β in the sciatic nerve of the CCI group were increased. Furthermore, the expression levels of cell death and pyroptosis-related genes in Schwann cells induced by LPS were increased compared with in the control group. In conclusion, an NP-related pyroptosis gene signature was constructed based on four pyroptosis-related genes and it was found that the expression of pyroptosis-related genes was upregulated in the early steps of the neuroinflammatory process in RSC96 cells.

Introduction

Neuropathic pain (NP) is pain caused by a somatosensory nerve system lesion or disease (1). A total of 6.9-10% of the world's population suffers from NP (2). Patients experience NP even after the initial stimulus has been removed (3). Since there is currently no effective clinical intervention for NP, it has become a serious global health challenge (4). Risk factors for NP include diabetes, nerve compression, traumatic factors, oxidative stress, cancer and inflammation (5). However, to the best of our knowledge, the molecular mechanisms associated with NP remain unclear; therefore, there is an urgent need to better understand these mechanisms. Pyroptosis depends on caspase-1 activation, is a unique mechanism of inflammation that regulates cell death and has been associated with several chronic inflammatory diseases (6,7). Gasdermin D (GSDMD) initiates the formation of pyroptosomes and caspase-1-mediated pyroptosis and forms membrane pores in the cell membrane to induce the release of pro-inflammatory cytokines and cell death (8). The pathogenesis of NP mainly occurs as follows: After a lesion is formed in the peripheral nerve, glial cell activation produces several pro-inflammatory mediators, resulting in an inflammatory response in the neural

Correspondence to: Professor Guoping Zhao or Dr Li Gao, College of Traditional Chinese Medicine, Jinan University, 601 Huangpu Avenue West, Guangzhou, Guangdong 510632, P.R. China
E-mail: tguo428@jnu.edu.cn
E-mail: li.gao@jnu.edu.cn

*Contributed equally

Abbreviations: NP, neuropathic pain; GEO, Gene Expression Omnibus; WGCNA, Weighted Gene Co-expression Network Analysis; GO, Gene Ontology; LASSO, least absolute shrinkage and selection operator; CCI, chronic constriction injury; GSEA, gene set enrichment analysis; GSDMD, gasdermin D; NLRC4, NLR family CARD domain containing 4; NAIP, neuronal apoptosis inhibitory protein; NLRP3, NLR family pyrin domain containing 3; LPS, lipopolysaccharide

Key words: neuropathic pain, pyroptosis, GEO, WGCNA

tissue (9,10). Inflammatory conditions, such as peripheral diabetic neuropathy, often cause the development of pyroptosis. However, to the best of our knowledge, only one study has investigated the role of pyroptosis in NP (11).

There are two types of cells in the peripheral nervous system, neurons and glial cells. Schwann cells are a type of glial cell (12). The role of Schwann cells in the peripheral nervous system is manifested in two ways: On the one hand, they physically support long axons, while on the other hand they release a variety of growth factors to nourish and form myelinated axons (13,14). After a lesion occurs in the peripheral nerve, Schwann cells undergo a phenotypical transformation into repair Schwann cells to promote nerve regeneration (15).

The present study aimed to identify NP-related pyroptosis genes, 50 samples from patients with NP and healthy volunteers were collected from the Gene Expression Omnibus (GEO) database and Weighted Gene Co-expression Network Analysis (WGCNA) was used for the identification of NP-related pyroptosis genes. Moreover, multivariate logistic regression was used to construct a pyroptosis-related gene signature. The expression levels of pyroptosis-related genes in lipopolysaccharide (LPS)-induced Schwann cells were examined by reverse transcription-quantitative PCR (RT-qPCR) and the cell death of LPS-induced Schwann cells was determined through flow cytometry.

Materials and methods

Data source. A total of two peripheral blood gene expression microarray datasets (GSE124272 and GSE150408) (16,17) for NP were obtained from the GEO database (https://www.ncbi.nlm.nih.gov/geo/). GSE124272 and GSE150408 were based on the same platform, GPL211. GSE124272 consisted of 8 patients with NP and 8 healthy volunteers. GSE150408 consisted of 17 patients with NP, 17 healthy volunteers and 17 treated patients. The 17 treated patients in the GSE150408 dataset were removed and then the GSE124272 and GSE150408 datasets were merged while the 'SVA' package (version 3.44.0; http://www.bioconductor.org/packages/release/bioc/html/sva.html) was used to remove batch effects from the merged datasets. Finally, a dataset containing 25 healthy volunteers and 25 patients with NP was obtained. The relative logarithmic expression boxplots reflect the consistency of the merged data (Fig. S1. A training (n=31) and a test cohort (n=19) were randomly split (6:4 ratio) from the pooled dataset. The test cohort was generated to assess the predictive power and robustness of prognostic-related risk models.

WGCNA. A gene co-expression network was constructed using the 'WGCNA' R package [version 1.71; https://cran.r-project.org/web/packages/WGCNA/index.html) (18)]. The height threshold cut-off was set to 230 and all samples were included in the present analysis (Fig. 1A). To build a scale-free network, β=8 (scale-free, R^2=0.9) was selected as the soft threshold. A weighted adjacency matrix was converted to a topological overlap matrix (TOM) to estimate network connectivity. The clustering tree structure of TOM was constructed using the hierarchical clustering method (18). The different colours of the cluster branches represent different gene modules. Finally, module membership (MM) and genetic significance (GS) were calculated to relate the modules to the clinical features (18,19).

Identification of pyroptosis-related genes in NP. Gene ontology (GO) enrichment analysis of NP-related module genes from the WGCNA was performed using the 'clusterProfiler' R package (version 4.4.4; http://www.bioconductor.org/packages/release/bioc/html/clusterProfiler.html) and NP-related module genes were overlapped with 49 pyroptosis-related genes (Table SI) (20-23). Venn diagrams were used to describe the details of gene overlap. Subsequently, the 'ggplot' R package (version 3.3.6; https://cran.r-project.org/web/packages/ggplot2/index.html) (24) was used to plot histograms of the differences in the expression levels of pyroptosis-related module genes in healthy volunteers and patients with NP.

Construction and validation of pyroptosis-related gene signature. Pyroptosis-related module genes were included in univariate logistic regression using the 'foreign' R package (version 0.8-83; https://cran.r-project.org/web/packages/foreign/index.html) and genes with P<0.05 were selected as prognosis-related pyroptosis genes. Subsequently, least absolute shrinkage and selection operator (LASSO) regression was performed using the 'glmnet' R package (version 4.1-4; https://cran.r-project.org/web/packages/glmnet/index.html), which compressed the regression coefficients to obtain a more refined model by including a penalty function (λ) in the regression model. A stepwise regression method was then used to construct a multiple logistic regression model for genes with regression coefficients >0. The risk score of each sample was then calculated according to the regression coefficient obtained by LASSO regression: $Risk\ score = \sum_{i=1}^{n} coef_i\, x_i$. The risk score for this model can be obtained from the following formula: Risk score=0.0519 x expression level of GSDMD + 0.0848 x expression level of NAIP + 0.0214 x expression level of NLRC4 + 0.2080 x expression level of NLRP3 (25).

Patients were divided into the high- and low-risk groups based on the median risk score. The receiver operating characteristic (ROC) curve generated using the 'ROC' R package (version 1.72.0; http://www.bioconductor.org/packages/release/bioc/html/ROC.html) was used to evaluate the predictive ability of the regression model.

Nomogram construction and verification. Nomograms were established based on factors identified by multivariate logistic regression analysis using the 'foreign' R package and a calibration curve was drawn to evaluate the accuracy of the multivariate logistic regression model. Multivariate logistic regression was evaluated by decision curve (DC) analysis using the 'rmda' R package (version 1.6; https://cran.r-project.org/web/packages/rmda/index.html), with a threshold probability of 0.1 for the DCs based on the incidence of the disease. Furthermore, the model was evaluated through the clinical impact curve (26).

Assessment of the level of immune cell infiltration in the high- and low-risk groups. Based on the CIBERSORT (https://cibersortx.stanford.edu/) algorithm, the infiltration levels of immune cells in the high- and low-risk groups were estimated. The proportions of 22 immune cells in the high and low-risk groups were obtained using the CIBERSORT

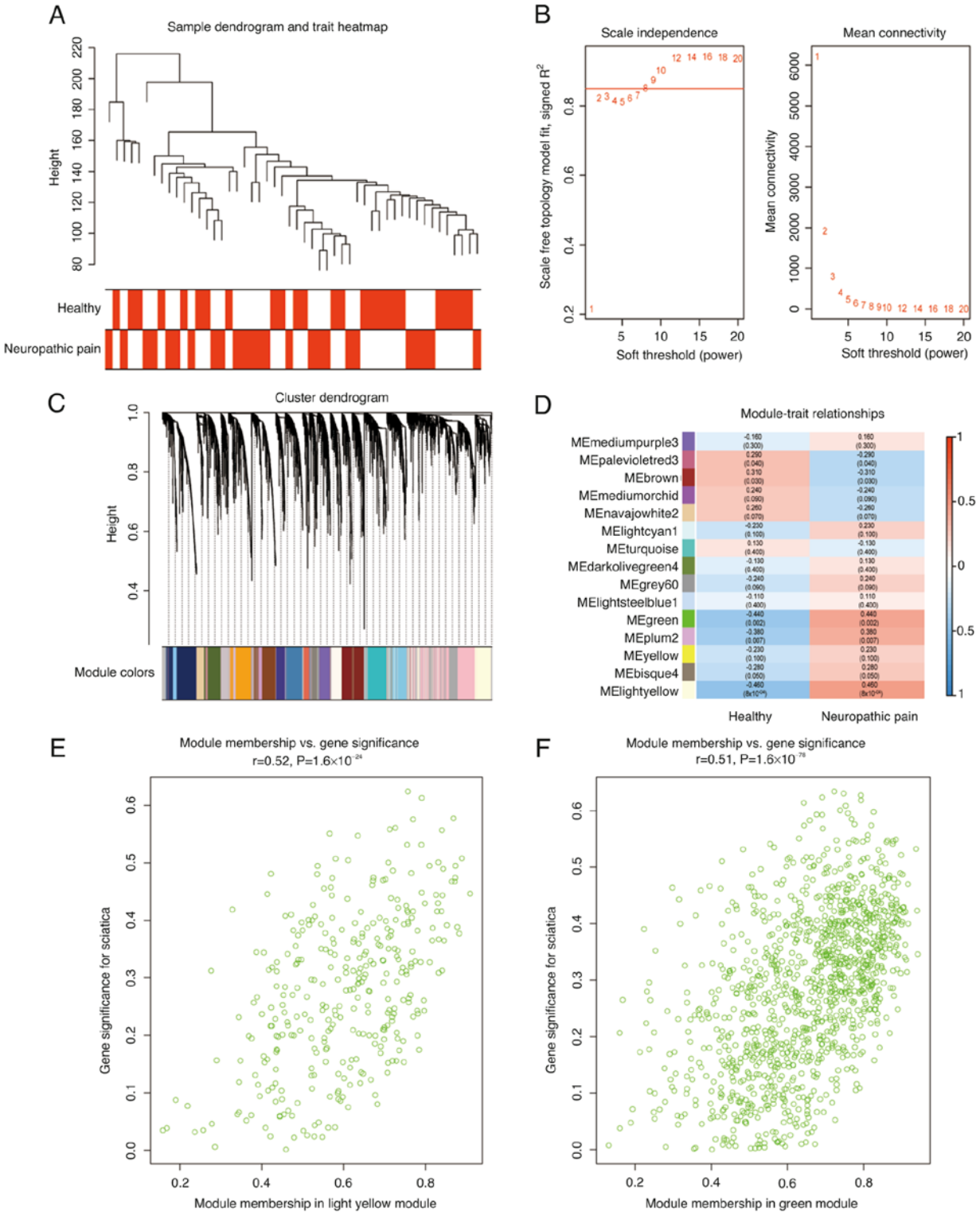

Figure 1. WGCNA results. (A) Cluster dendrogram of clinical characteristics and data from 50 patients with NP and healthy controls. (B) Scale-free fit index for soft-thresholding powers. The soft-thresholding power in the WGCNA was determined based on a scale-free R^2 (R^2=0.90). The left panel presents the relationship between the soft-threshold and scale-free R^2. The right panel presents the relationship between the soft-threshold and mean connectivity. (C) Dendrogram of the differentially expressed genes clustered based on different metrics. Each branch in the figure represents one gene and each colour below represents one co-expression module. (D) Heatmap of correlations between MEs and clinical characteristics of patients with NP. Each cell contains the correlation coefficient and P-value. (E) GS score and MM scatter plot for genes in the light yellow module. (F) GS score and MM scatter plot for genes in the green module. WGCNA, Weighted Gene Co-expression Network Analysis; MEs, module eigengenes; NP, neuropathic pain; GS, genetic significance; MM, module membership.

algorithm. They were then visualized using the 'ggplot2' and 'ggpubr' packages (version 0.4.0; https://cran.r-project.org/web/packages/ggpubr/index.html).

Gene set enrichment analysis (GSEA). GSEA was performed using the expression matrix grouped by risk score on GSEA 4.2.1 software (Broad Institute of MIT and Harvard;

http://www.gsea-msigdb.org/gsea/index.jsp) and the reference gene set was selected as h.all.v7.5.1.symbols.gmt [Hallmarks]. The pathways were assessed using normalized P-values ($P<0.05$) and enrichment scores.

Reagents. Evo M-MLV RT-PCR Kit, SYBR® Green Pro Taq HS Master Mixed qPCR Kit and RNase Free water (cat. nos. AG11602, AG11701 and AG11012, respectively) were acquired from Accureate Biology. LPS ELISA kit (cat. no. MM-0647R1) was purchased from Lvye Biotechnology Co., Ltd. and LPS (cat. no. L2880) was purchased from MilliporeSigma. H&E (cat. no. GL1005) and toluidine blue (cat. no. GP1052) reagents were acquired from Wuhan Servicebio Technology Co., Ltd. The rabbit polyclonal S100 calcium-binding protein β (S100β; cat. no. GB13359) (https://www.service-bio.cn/goodsdetail?id=1185) antibodies were obtained from Wuhan Servicebio Technology Co., Ltd. and ionized calcium-binding adapter molecule 1 (Iba-1; cat. no. A5595) antibodies were obtained from Bimake Biotechnology Co., Ltd. A goat anti-rabbit secondary antibody for immunohistochemistry (cat. no. G1213) was acquired from Wuhan Servicebio Technology Co., Ltd.

Animals. A total of 18 male Sprague Dawley rats weighing 180-230 g and aged 7-8 weeks were acquired from Beijing Huafukang Biotechnology Co., Ltd. The rats were randomly divided into sham-operated and chronic constriction injury (CCI) groups. Rats were housed in standard plastic cages at 24±1˚C and 50-70% humidity. Rats were kept on a 12/12 h light-dark cycle in the animal environment with free access to water and food. All animal experiments were conducted following the guidelines established by the National Academy of Sciences, the National Institutes of Health and the Institute of Laboratory Animal Resources (US). All experimental protocols were approved by the Animal Ethics Committee of Jinan University (Guangzhou, China; approval no. IACUC-20200115-04).

Sciatic nerve injury model and groups. Based on previous studies, CCI of the sciatic nerve was chosen as the disease model for NP (27,28). The right sciatic nerve of rats was exposed following an intraperitoneal injection of sodium pentobarbital (3%; 40 mg/kg) and it was ligated under a microscope using 4.0 sutures (repeated four times at ~1 mm intervals). The rats in the sham group were not subjected to nerve ligation. To prevent infection, gentamicin (10 mg/ml) was injected into the right biceps femoris muscle. A total of 18 rats were randomized into two groups, the CCI and the sham operation group. After 21 days, the rats were sacrificed by exsanguination after excessive anaesthesia (200 mg/kg sodium pentobarbital).

H&E and toluidine blue staining. Sciatic nerve tissues were fixed in 4% paraformaldehyde for 1 day at room temperature, paraffin-embedded, and sliced at a thickness of 3 μm. Sections were deparaffinized with xylene for 15 min at room temperature and rehydrated with 100, 90, 80 and 70% ethanol for 5 min at room temperature. After washing with PBS for 5 min, the specimens were stained with H&E or toluidine blue for 5 min at room temperature, thereafter these were washed with water or incubated with glacial acetic acid, respectively. Images were observed by two different pathologists who were unaware of the experiment (BX53 fluorescence microscope; Olympus Corporation).

Immunohistochemistry and ELISA on the sciatic nerve model. The right sciatic nerve was fixed in 4% paraformaldehyde for 24 h at room temperature, immersed in 20% (w/v) sucrose solution for 5 min at room temperature sectioned at a thickness of 9 μm and then incubated in sodium citrate antigen retrieval solution (1 mM EDTA; 1:1,000; pH=6) for 5 min at room temperature. Subsequently the tissue was blocked with 3% BSA (cat. no. G5001; Wuhan Servicebio Technology Co., Ltd.) for 30 min at room temperature. The sections were then incubated with rabbit Iba1 (1:50) and S100β (1:500) antibodies overnight at 4˚C, followed by goat anti-rabbit secondary antibody (1:200) for 50 min at room temperature. The sections were rinsed with DAB developer solution and counterstained with hematoxylin for ~3 min. Finally, the sections were dehydrated in an ascending alcohol series, cleared with xylene. and sealed. The slices were observed under an OLYMPUS fluorescence microscope (BX53; Olympus Corporation). The mean density was calculated using Image-Pro Plus software (Media Cybernetics, Inc.) and statistical analysis was performed.

The serum was centrifuged at 1,500 x g for 10 min at 4˚C and 600 μl of the supernatant was aspirated for the analysis of LPS levels via ELISA, according to the manufacturer's instructions.

Culture and treatment of Schwann cells. RSC96 cells, a spontaneously immortalized rat Schwann cell line derived from the long-term culture of rat primary Schwann cells, were purchased from the Shanghai Institute of Cell Biology. The cells were cultured in high glucose Dulbecco's modified Eagle's medium (Gibco; Thermo Fisher Scientific, Inc.) containing 10% fetal bovine serum (Shanghai Baisai Biotechnology Co., Ltd.) and antibiotics (penicillin and streptomycin; 1%) at 37˚C in a 5% CO_2 humidified atmosphere. Cells were seeded in 6-well dishes at a density of $1x10^6$ per well and were then treated with LPS (10 μM/ml) in a 37˚C incubator for 24 h, whereas cells in the control group were left untreated.

Cell death assay. For the assessment of Schwann cell mortality, Annexin V-Alexa fluor 647 and PI (cat. no. AP006-100; Shanghai Yishan Biotechnology Co., Ltd.) staining was performed. LPS-treated cells were harvested with trypsin, Briefly, $1x10^6$ cells/ml were centrifuged at 350 x g for 10 min at 4˚C, the supernatant was discarded and 1 ml cold PBS was added and agitated gently to suspend the cells, prior to further centrifugation at 350 x g for 10 min at 4˚C. The supernatant was discarded, the cells were resuspended in 200 μl binding buffer, and incubated with 10 μl Annexin V-Alexa fluor 647 and PI at room temperature for 15 min. Finally, cells were analysed using a CytoFLEX flow cytometer and CytExpert 2.3 (both from Beckman Coulter, Inc.). In the plots, quadrant (Q)4 shows surviving cells, Q2 and Q3 show dead cells, and Q1 show cell debris; Q2 and Q3 were used to assess apoptosis.

RNA extraction, cDNA synthesis and RT-qPCR. Total RNA was extracted from the treated and untreated RSC96 cells using RNAiso Plus (Accureate Biology) and reverse-transcribed to

Table I. Primer sequences used for reverse transcription-quantitative PCR.

Gene	Forward primer	Reverse primer
β-actin	5'-CCTAGACTTCGAGCAAGAGA-3'	5'-GGAAGGAAGGCTGGAAGA-3'
Gasdermin D	5'-AGACATCGGGAGGATTTTAC-3'	5'-GAGCACCAGACACTCAAGG-3'
NLR family pyrin domain containing 3	5'-CTGTCTCACATCTGCGTGTT-3'	5'-GTCTCCCAAGGCATTTTCT-3'
Caspase-1	5'-TGAAAGACAAGCCCAAGGT-3'	5'-GAAGAGCAGAAAGCAATAAAA-3'
IL-18	5'-CTGGCTGTGACCCTATCTG-3'	5'-AAGCATCATCTTCCTTTTGG-3'
IL-1β	5'-AGGAGAGACAAGCAACGACA-3'	5'-CTTTTCCATCTTCTTCTTTGGGTAT-3'

cDNA using Evo M-MLV RT-PCR Kit (Accureate Biology). RT was performed at 37˚C for 15 min and 85˚C for 5 sec, according to the manufacturer's instructions. The following thermocycling conditions were used for qPCR: Initial denaturation at 95˚C for 1 min; 40 cycles of 95˚C for 10 sec and 60˚C for 30 sec. The mRNA levels were quantified using the $2^{-\Delta\Delta Cq}$ method and normalized to the internal reference gene β-actin (29). The primer pairs used for qPCR are listed in Table I.

Statistical analysis. Each experiment was repeated successfully at least in triplicate. Statistical data are presented as the mean ± SEM. Group differences were analysed using either the Mann-Whitney U test or a two-tailed unpaired Student's t-test. Odds ratios (ORs) and 95% CIs were calculated using logistic regression models. P<0.05 was considered to indicate a statistically significant difference. R 4.0.2 software (https://www.r-project.org/) was used for data processing and statistical analysis.

Results

Construction of a WGCN. Firstly, the samples were clustered to assess them for significant outliers. Subsequently, the 'WGCNA' R package was used to construct the gene co-expression network (Fig. 1B). A weighted adjacency matrix was converted to a TOM to estimate network connectivity. The hierarchical clustering method was used to construct the clustering tree structure of TOM. Cluster tree branches represent different gene modules in different colours. Ultimately, a total of 87 modules were obtained (Fig. 1C). The GS and MM were then calculated to identify the association between modules and disease. The highest association with the disease was found in the light yellow (r=0.46) and green (r=0.44;) modules (Fig. 1D). Significant correlations between green and light yellow MM and GS are shown in Fig. 1E and F.

Functional enrichment analysis in modules of interest. The 'clusterProfiler' R package was used to perform GO enrichment analysis for genes in the light yellow (Table SII) and green (Table SIII) modules. The genes in the light yellow module were not enriched for any molecular function and biological process but only enriched for cellular components (Table II), including the 'cytoplasmic side of plasma membrane', 'cytoplasmic side of membrane', 'extrinsic component of membrane', 'secretory granule lumen', 'cytoplasmic vesicle lumen', 'vesicle lumen' and 'nuclear membrane' (Fig. 2A). The results of GO enrichment analysis of the genes in the green module showed that their main biological functions focused on the immune response of neutrophils and the production of cytokines. Moreover, pyroptosis-related genes were significantly enriched in 'neutrophil-mediated immunity', 'neutrophil activation', 'neutrophil degranulation', 'neutrophil activation involved in immune response' as well as 'positive regulation of cytokine production' (Fig. 2B; Table II). Since the enrichment analysis results for the genes in the yellow module were not very clear, these were not included in the subsequent analyses.

Overlapping NP-related genes with pyroptosis-related genes. WGCNA-derived NP-related module genes were overlapped with 51 pyroptosis-related genes and six overlapping genes were obtained, namely pyroptosis-related module genes, as shown in the Venn diagram (Fig. 2C). These genes included GSDMD, IL-1β, neuronal apoptosis inhibitory protein (NAIP), NLR family CARD domain containing 4 (NLRC4), NLR family pyrin domain containing 3 (NLRP3) and Tet methylcytosine dioxygenase 2. The expression differences of these genes were examined between healthy controls and patients with NP and it was found that only GSDMD, NLRP3, NAIP and NLRC4 were upregulated in patients with NP (Fig. 2D).

Identification of genes in the pyroptosis-related module and construction of risk scoring models. Based on the univariate logistic regression analysis of six module genes associated with pyroptosis, four genes closely associated with NP were identified, namely GSDMD (P=0.034), NAIP (P=0.026), NLRC4 (P=0.025) and NLRP3 (P=0.010). The OR for these four genes was >1 (Fig. 3A), suggesting that these genes were associated with an increased risk of disease. The LASSO algorithm was then used to compress the regression coefficients to eliminate multicollinearity among the four variables and prevent model overfitting. The optimal penalty parameter (λ=0.06013478) for the LASSO model was determined by 10-fold cross-validation (Fig. 3B and C). These four genes were then integrated into a multivariate logistic regression to construct a diagnostic pyroptosis-related gene signature. Subsequently, patients with NP were divided into two distinct risk groups based on the median risk score: High risk (n=13) and low risk (n=12).

Validation of prognostic models. Predictive effects of pyroptosis-related gene signatures were assessed using ROC

Table II. Gene Ontology enrichment analysis of light yellow and green module genes.

Module	Term	ID	Description	P-value
Light yellow	CC	GO:0009898	Cytoplasmic side of plasma membrane	$1.03x10^{-5}$
Light yellow	CC	GO:0098562	Cytoplasmic side of the membrane	$2.51x10^{-5}$
Light yellow	CC	GO:0031234	Extrinsic component of cytoplasmic side of plasma membrane	$1.43x10^{-4}$
Light yellow	CC	GO:0019897	Extrinsic component of plasma membrane	$1.22x10^{-3}$
Light yellow	CC	GO:0019898	Extrinsic component of membrane	$1.39x10^{-3}$
Light yellow	CC	GO:0005834	Heterotrimeric G-protein complex	$1.39x10^{-3}$
Light yellow	CC	GO:1905360	GTPase complex	$1.39x10^{-3}$
Green	BP	GO:0002446	Neutrophil-mediated immunity	$6.46x10^{-33}$
Green	BP	GO:0042119	Neutrophil activation	$6.46x10^{-33}$
Green	BP	GO:0043312	Neutrophil degranulation	$1.38x10^{-32}$
Green	BP	GO:0002283	Neutrophil activation involved in immune response	$1.71x10^{-32}$
Green	BP	GO:0001819	Positive regulation of cytokine production	$1.83x10^{-8}$
Green	BP	GO:0032675	Regulation of interleukin-6 production	$6.71x10^{-6}$
Green	BP	GO:0032635	Interleukin-6 production	$9.51x10^{-6}$
Green	BP	GO:0032680	Regulation of tumour necrosis factor production	$2.94x10^{-5}$
Green	BP	GO:0032640	Tumour necrosis factor production	$3.30x10^{-5}$
Green	BP	GO:1903555	Regulation of tumour necrosis factor superfamily cytokine production	$3.74x10^{-5}$
Green	BP	GO:0071706	Tumour necrosis factor superfamily cytokine production	$4.77x10^{-5}$
Green	BP	GO:1901653	Cellular response to peptide	$6.55x10^{-5}$
Green	BP	GO:0042326	Negative regulation of phosphorylation	$1.63x10^{-4}$
Green	BP	GO:0002755	Myd88-dependent toll-like receptor signalling pathway	$1.63x10^{-4}$
Green	MF	GO:0051213	Dioxygenase activity	$1.49x10^{-3}$
Green	MF	GO:0038187	Pattern recognition receptor activity	$3.30x10^{-3}$
Green	MF	GO:0003953	NAD^+ nucleosidase activity	$3.30x10^{-3}$
Green	MF	GO:0050135	$NAD(P)^+$ nucleosidase activity	$3.30x10^{-3}$
Green	MF	GO:0061809	NAD^+ nucleosidase, cyclic ADP-ribose generating	$3.30x10^{-3}$
Green	MF	GO:0140375	Immune receptor activity	$3.36x10^{-3}$
Green	CC	GO:0030667	Secretory granule membrane	$3.88x10^{-16}$
Green	CC	GO:0070820	Tertiary granule	$3.58x10^{-15}$
Green	CC	GO:0042581	Specific granule	$5.43x10^{-14}$
Green	CC	GO:0101002	Ficolin-1-rich granule	$1.05x10^{-13}$
Green	CC	GO:0070821	Tertiary granule membrane	$2.25x10^{-08}$
Green	CC	GO:0035579	Specific granule membrane	$1.26x10^{-07}$
Green	CC	GO:0034774	Secretory granule lumen	$2.63x10^{-07}$
Green	CC	GO:0060205	Cytoplasmic vesicle lumen	$3.23x10^{-07}$
Green	CC	GO:0031983	Vesicle lumen	$3.38x10^{-07}$
Green	CC	GO:0101003	Ficolin-1-rich granule membrane	$3.66x10^{-07}$

CC, cellular component; BP, biological process; MF, molecular function.

curves. The samples from patients with NP were randomly divided into the training and validation sets at a ratio of 6:43 and then the ROC curves of the training set, validation set and of all samples were plotted. The results showed that the area under the curve of the training, validation and all sample sets was 0.755, 0.821 and 0.746, respectively (Fig. 3D-F), which showed that the model had a satisfactory prediction performance.

Construction of nomogram model. To facilitate the use of selected pyroptosis-related module genes (GSDMD, NLRP3, NAIP and NLRC4) by clinicians for the diagnosis of NP, OR values of pyroptosis-related module genes are shown in Fig. 4A. a nomogram model was constructed (Fig. 4B). The calibration curve showed that the positive rate of the nomogram model in diagnosing NP was consistent with the actual positive rate (Fig. 4C). Although the DC showed that there was not much difference in the net benefit of the model constructed by a single gene and the model constructed by the overall four genes (Fig. 4D), the clinical impact curve analysis showed that the diagnostic ability of the model constructed by the overall four genes was relatively high (Fig. 4E).

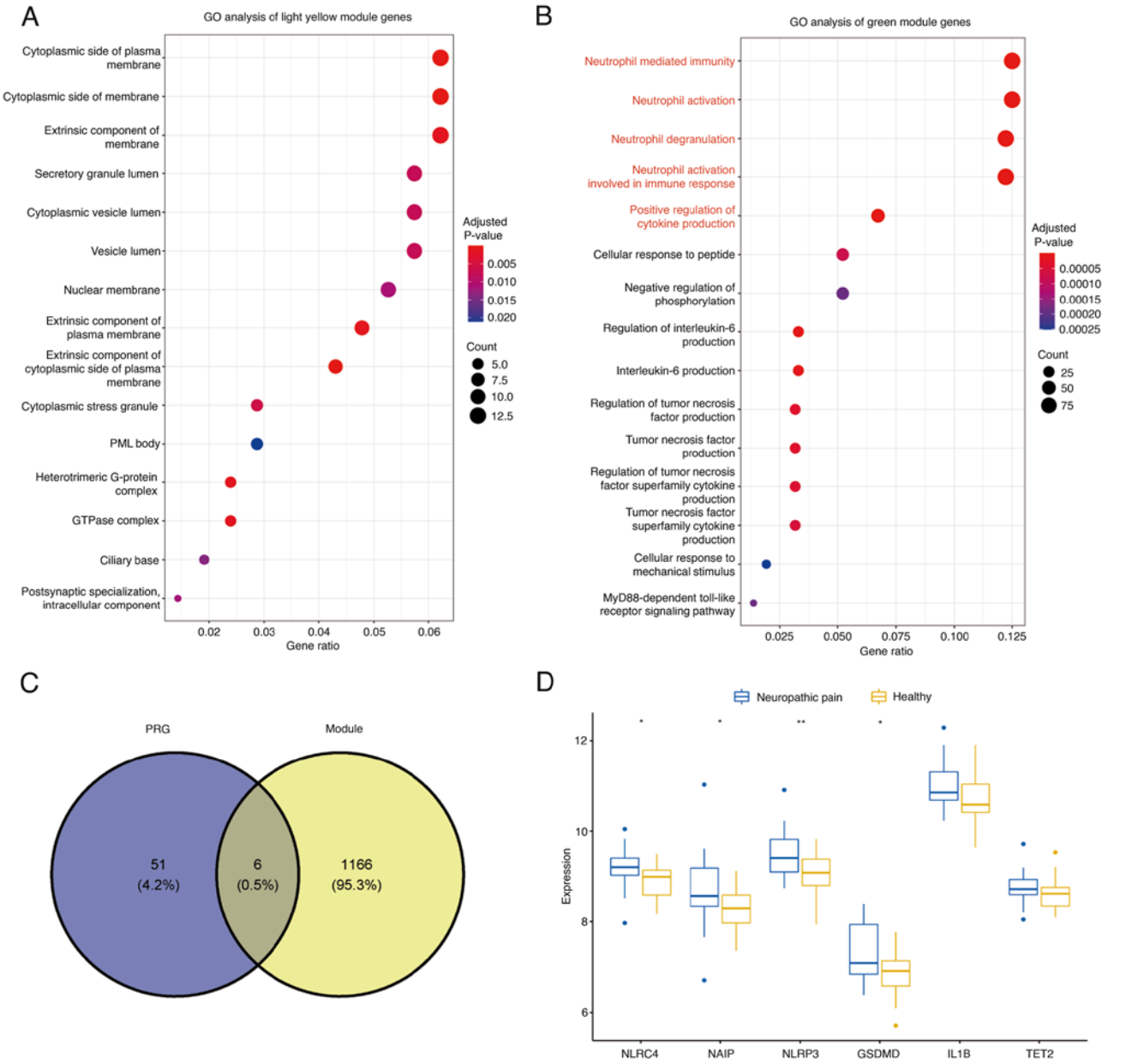

Figure 2. Identification and analysis of key module and pyroptosis-related module genes. (A) GO analysis of light yellow module. (B) GO analysis of green module (biological processes marked in red are the most enriched in pyroptosis signatures). (C) Venn diagram of the intersection of 51 pyroptotic genes with genes in the green module. (D) Differences in the expression levels of pyroptosis-related module genes and genes of the classical pyroptosis pathway between healthy individuals and patients with neuropathic pain. *P<0.05 and **P<0.01. GO, gene ontology; GSDMD, gasdermin D; NAIP, neuronal apoptosis inhibitory protein; NLRC4, NLR family CARD domain containing 4; NLRP3, NLR family pyrin domain containing 3; CASP1, caspase-1; TET2, Tet methylcytosine dioxygenase 2.

Immune cell infiltration levels and GSEA in the high- and low-risk groups. The differences in the level of immune cell infiltration between the high- and low-risk groups were further studied and it was found that there were higher infiltration levels of macrophages, central memory CD8 T cells, and activated dendritic cells in the high-risk group compared with in the low-risk group (Fig. 5A and B). The GSEA results (Fig. 5C) showed that 'IL-6_JAK_STAT3 signaling', 'inflammatory response', 'interferon-α response', 'interferon-γ response', 'mitotic spindle', 'Notch signaling', 'TGF-β signaling' and other signaling pathways were upregulated in the high-risk group, and these signaling pathways were associated with inflammation and non-specific immune response.

H&E staining, toluidine blue staining, immunohistochemical analysis and ELISA on the sciatic nerve injury model. To further explore the role of pyroptosis in NP, a CCI model was generated. On day 21, sciatic nerve tissue was visualized both through H&E and toluidine blue staining. Infiltration of inflammatory cells in the CCI model group was observed following H&E staining (Fig. 6A). Following toluidine blue staining, a normal neurological outcome could be observed in the sham group, while destruction of the normal neurological outcome and the disappearance of myelin sheath could be observed in the CCI model group (Fig. 6B). S100β is a Ca^{2+} binding protein present in glial cells, mainly in Schwann cells and satellite glial cells in peripheral nerves (30). Immunohistochemical

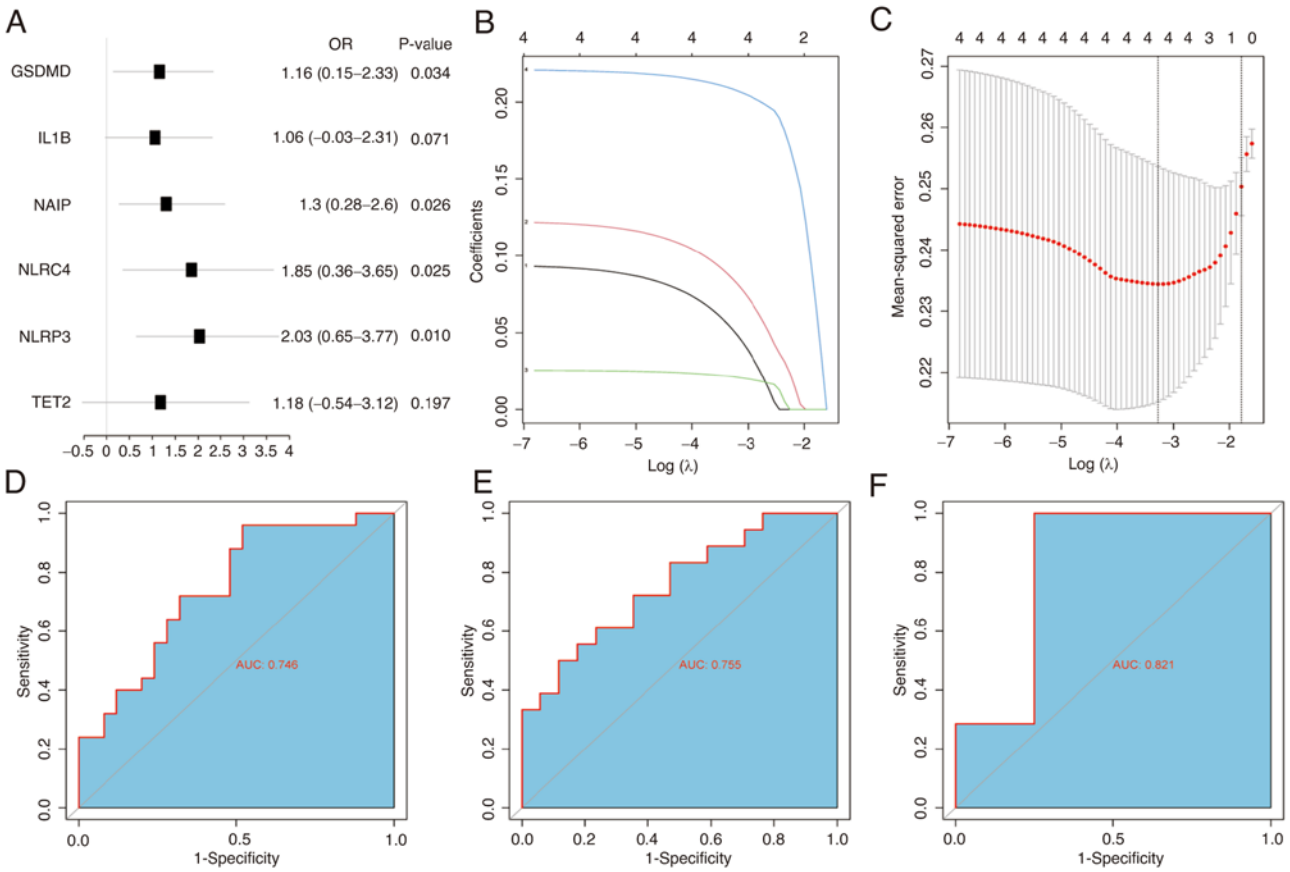

Figure 3. Construction of a diagnostic pyroptosis-related gene signature. (A) Forest plot of univariate logistic regression analysis of NPs for each pyroptosis-related module gene. (B) Distribution of LASSO coefficients of four pyroptosis-related module genes. (C) The 10-fold cross-validation for variable selection in LASSO models. Receiver operating characteristic curves of the (D) entire, (E) training and (F) test cohorts. NP, neuropathic pain; LASSO, least absolute shrinkage and selection operator; AUC, area under the curve; GSDMD, gasdermin D; NAIP, neuronal apoptosis inhibitory protein; NLRC4, NLR family CARD domain containing 4; NLRP3, NLR family pyrin domain containing 3; TET2, Tet methylcytosine dioxygenase 2; OR, odds ratio.

analysis showed that in normal sciatic nerves, S100β was mainly distributed in the myelin sheath, while the level of S100β in the CCI model group was significantly lower than that in the sham operation group (Fig. 6C). Iba-1 is expressed by cells of the microglia/macrophage lineage and Iba-1 expression is increased in activated microglia (31). The results of the CIBERSORT analysis showed that macrophages had higher infiltration levels in the high-risk group, while the immunohistochemical analysis showed that the level of Iba-1 in the CCI model group was significantly higher than that in the control group (Fig. 6D).

LPS-induced pyroptosis in Schwann cells. Toluidine blue staining showed that the sciatic nerve in the CCI model group was demyelinated, the integrity of its myelin sheath was destroyed and decreased expression of S100β was observed in the CCI model, suggesting that the role of pyroptosis in NP may be related to Schwann cell pyroptosis. Therefore, further cell experiments were performed to examine the pyroptosis of RSC96 Schwann cells. Flow cytometry showed that LPS induced RSC96 cell death (Fig. 7A). The expression levels of pyroptosis-related genes in RSC96 cells induced by LPS were detected using RT-qPCR and it was found that GSDMD, NLRP3, caspase-1, IL-1 and IL-18 has a higher mRNA expression level in LPS-induced RSC96 cells compared with in the control group (Fig. 7B). Consistently, the serum levels of LPS, an inflammatory factor, were significantly increased in the CCI group compared with the Sham group (Fig. 7C).

Discussion

The present study identified NP-related pyroptosis genes through bioinformatic analysis and found that Schwann cell pyroptosis occurs during neuroinflammation. The major findings were as follows: i) A total of four pyroptosis-related genes (GSDMD, NLRP3, NAIP and NLRC4) increase the risk of NP; ii) a four-gene risk signature was developed; iii) macrophages exhibit higher infiltration levels in high-risk patients with NP compared with low-risk patients; and iv) Schwann cells undergo pyroptosis in a neuroinflammatory environment.

Inflammation due to intracellular or extracellular stimuli, such as viruses, toxins and bacteria, can lead to the development of pyroptosis. Pyroptosis is a type of programmed cell death during which GSDMD forms membranous pores in the cell membrane (32). When the body is stimulated by external factors causing damage, the inflammasome assembles and activates caspase-1 which cleaves and thereafter activates GSDMD. Activated GSDMD is then translocated to the membrane to form a pore, releasing mature IL-1β and IL-18 and causing cell swelling and cytoplasmic efflux, eventually leading to cell membrane rupture and pyroptosis (33).

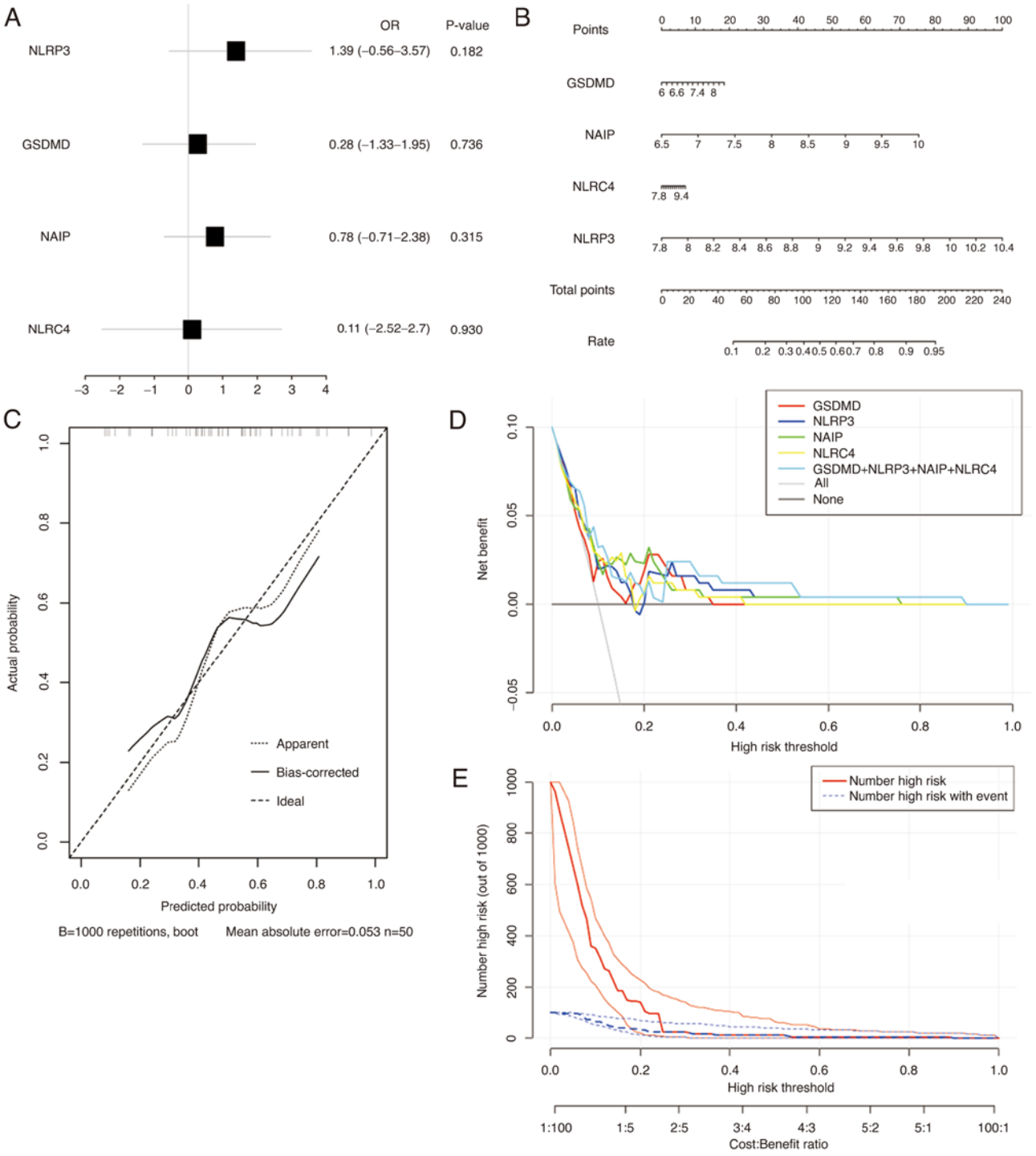

Figure 4. Construction of nomogram. (A) Forest plot of multivariate logistic regression analysis of four pyroptosis-related module genes. (B) Construction of nomogram based on selected pyroptosis-related module genes (GSDMD, NAIP, NLRC4 and NLRP3). (C) Calibration curve showing the diagnostic capability of the nomogram model. (D) Decision curves of the logistic regression model composed of a single or four pyroptosis-related module genes. (E) Clinical impact curve shows that the difference between the predicted positive rate and the true positive rate of nomogram mode was very small, indicating that nomogram mode can effectively predict the occurrence of neuropathic pain.

Numerous studies have demonstrated that NLRPs, including NLRC4, NLRP1, NLRP3, NLRP7 and NLRP12 and other inflammasomes, are involved in the onset and development of NP (34,35). Earlier studies have shown that the activation of the NLRP3 inflammasome contributes to mechanical allodynia in lumbar disc hernia, painful neuropathy caused by bortezomib and type 2 diabetic neuropathy (36-38), demonstrating that pyroptosis is essential to the development of NP.

The four genes (GSDMD, NLRP3, NAIP and NLRC4) were included in a nomogram model. The NLRP3 inflammasome consists of three parts, caspase-1, the adaptor protein apoptosis-associated speck-like protein with caspase activation and recruitment domain, as well as the receptor protein NLRP3 (39). The activation of the NLRP3 inflammasome is different from that of other inflammasomes. In addition to its activation by toxins, adenosine 5'-triphosphate or LPS (40),

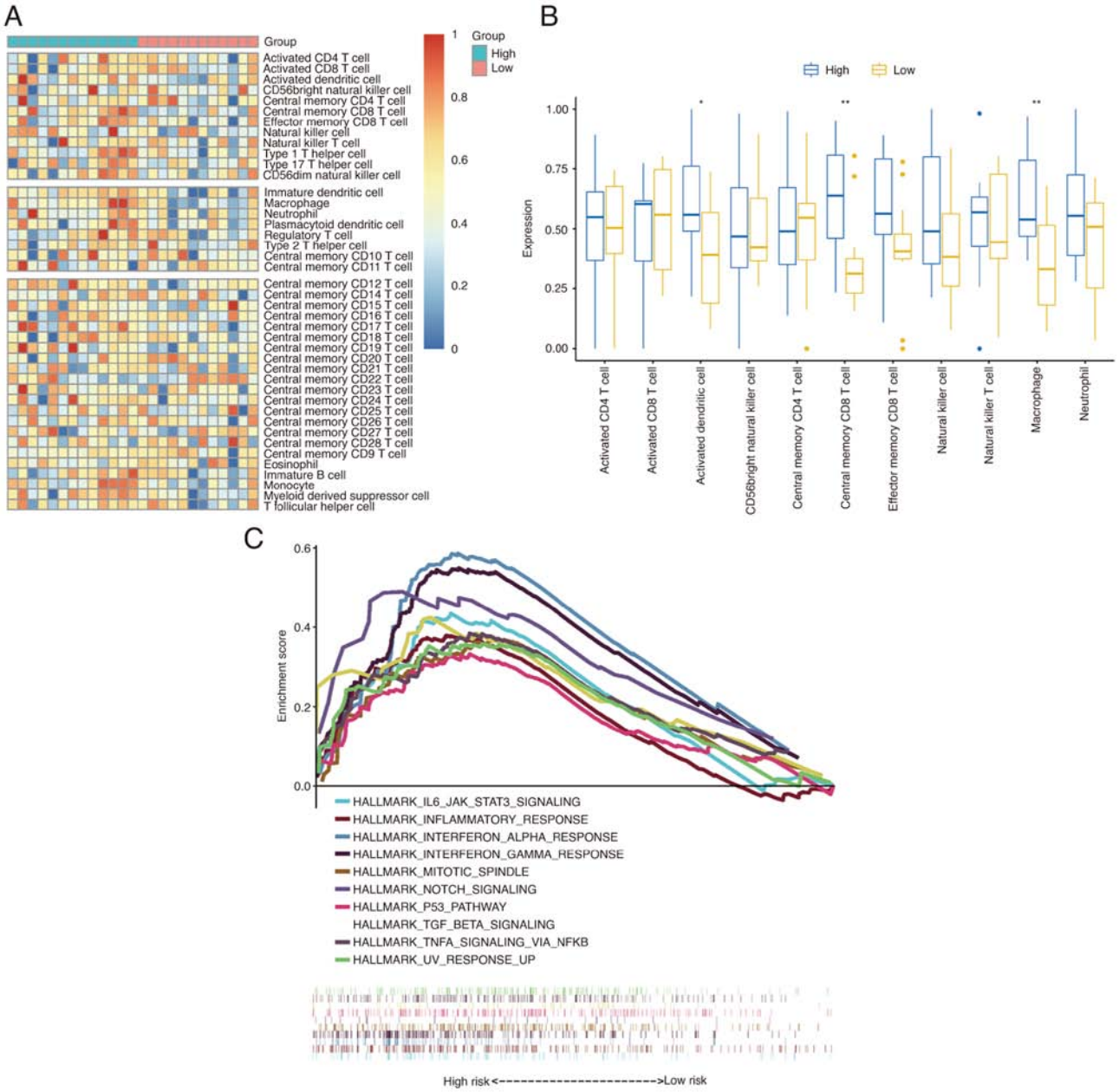

Figure 5. GSEA and immune infiltration analysis in the high- and low-risk groups. (A) Heatmap of ssGSEA scores for 42 immune cell types in high- and low-risk groups. (B) Boxplot of ssGSEA scores between high-risk and low-risk groups, the results of which show that activated dendritic cells, central memory CD8 T cells and macrophages exhibited higher ssGSEA scores in the high-risk group. *P<0.05 and **P<0.01. (C) GSEA results of the high-risk and low-risk groups. GSEA, gene set enrichment analysis; ssGSEA, single-sample GSEA.

the activation of NLRP3 requires several molecular and cellular events as triggers, including reactive oxygen species, release of mitochondrial function barriers, K^+ efflux and Ca^{2+} signaling (41-45). Following peripheral nerve injury, inflammatory mediators are released from infiltrating immune cells and exert their influence on receptors and ion channels present in nociceptors through multiple second messenger pathways. Inflammation-induced peripheral nerve sensitization (46) results in post-translational modification of ion channels, leading to changes in their kinetics and activation thresholds (47). This results in the increased sensitivity and excitability of nociceptor terminals (48) ultimately mediating Ca^{2+} influx, which leads to the activation of the NLRP3 inflammasome (45,49). Moreover, NAIP proteins recognize microbial pathogens and then recruit NLRC4 proteins to the inflammasome (50). Several studies have shown that, in the development of sterile neuroinflammation, the expression level of NLRC4 is increased in astrocytes and microglia and that NLRC4 and NLRP3 act synergistically to induce neuronal cell death (48). As a key protein in mediating pyroptosis, GSDMD can be cleaved by activated caspase-1 to form two fragments, one consisting an active N-terminal kinase (GSDMD-NT) and the other a C-terminal kinase (51). In addition, GSDMD-NT causes cell membrane perforation and programmed cell death, prompting cells to release a series of inflammatory factors (52). GSDMD-NT binds to cell membrane components, such as phosphatidylserine, phosphatidylinositol and phosphatidic acid, and oligomerizes

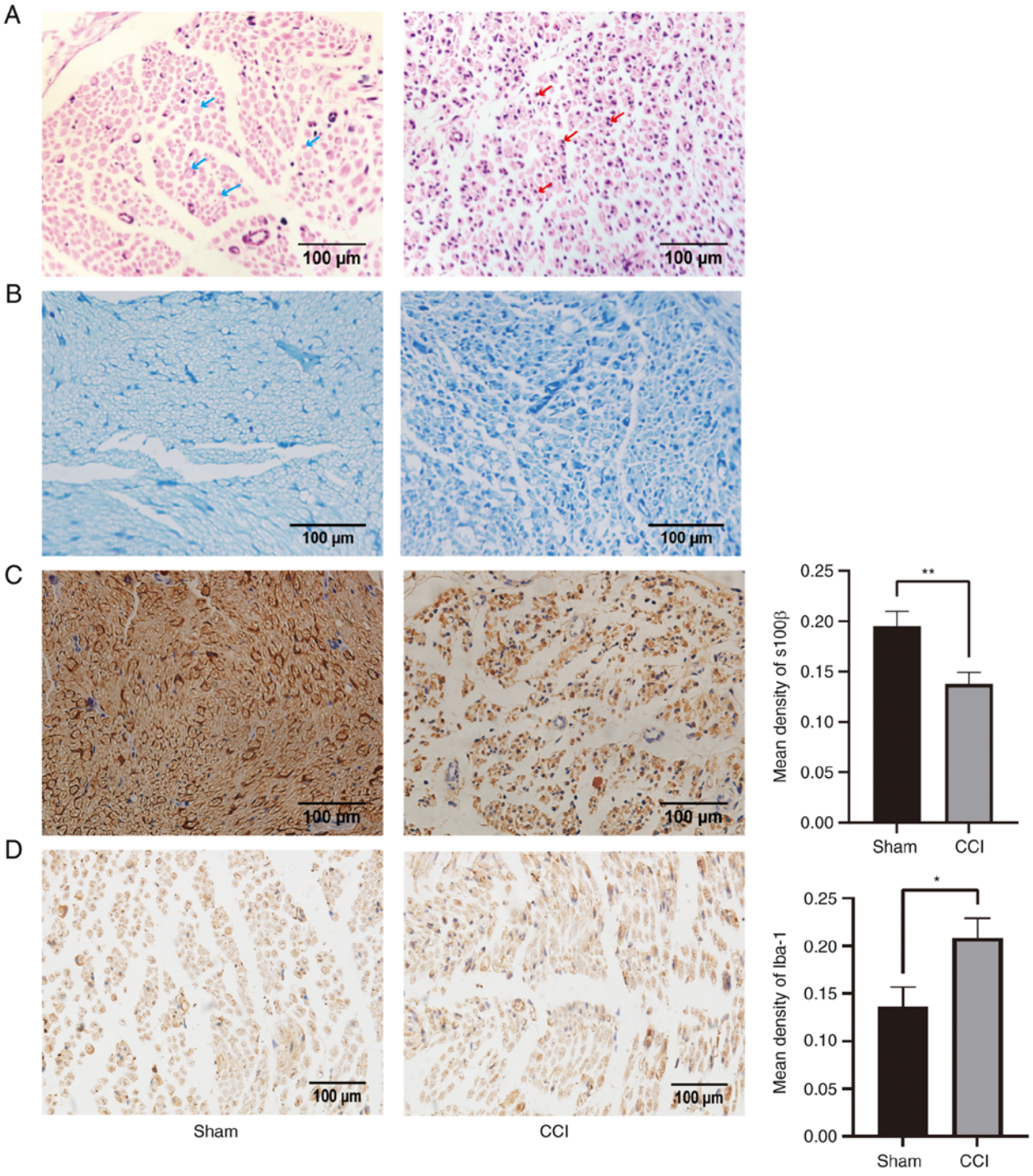

Figure 6. H&E, toluidine blue staining and immunohistochemistry. (A) H&E staining of the sham-operated (left image) (blue arrows indicate intact nerve myelin structures) and CCI (right image) groups (red arrows indicate inflammatory cells). (B) Toluidine blue staining of the sham-operated (left image) and CCI (right image) groups. Immunohistochemistry for (C) S100β and (D) Iba-1. Iba-1, ionized calcium-binding adapter molecule 1; CCI, chronic contraction injury; S100β, S100 calcium-binding protein β. *P<0.05 and **P<0.01.

to form a pore with a diameter of 10-15 nm in the cell membrane.

Peripheral nerve damage triggers the degradation of axons, leading to Wallerian degeneration (53), which leads to the dedifferentiation of Schwann cells and their separation from axons. Schwann cells can then respond to peripheral nerve injury through adaptive intracellular reprogramming, resulting in cells specialized in neural repair (54). These repairing Schwann cells produce neurotrophic factors to help neurons repair, and subsequently proliferate and migrate to form 'Büngner bands' that promote axonal growth (55). In response to nerve injury, cytokines, such as TNF-α, IL-1 and IL-6D, are produced and released by activated Schwann cells to recruit immune cells, contributing to axonal injury and enhancing nociceptor activity (56). In addition, activated Schwann cells secrete chemokines to induce macrophages to infiltrate the lesion and induce allodynia by activating transient receptor potential cation channel subfamily A member 1 on

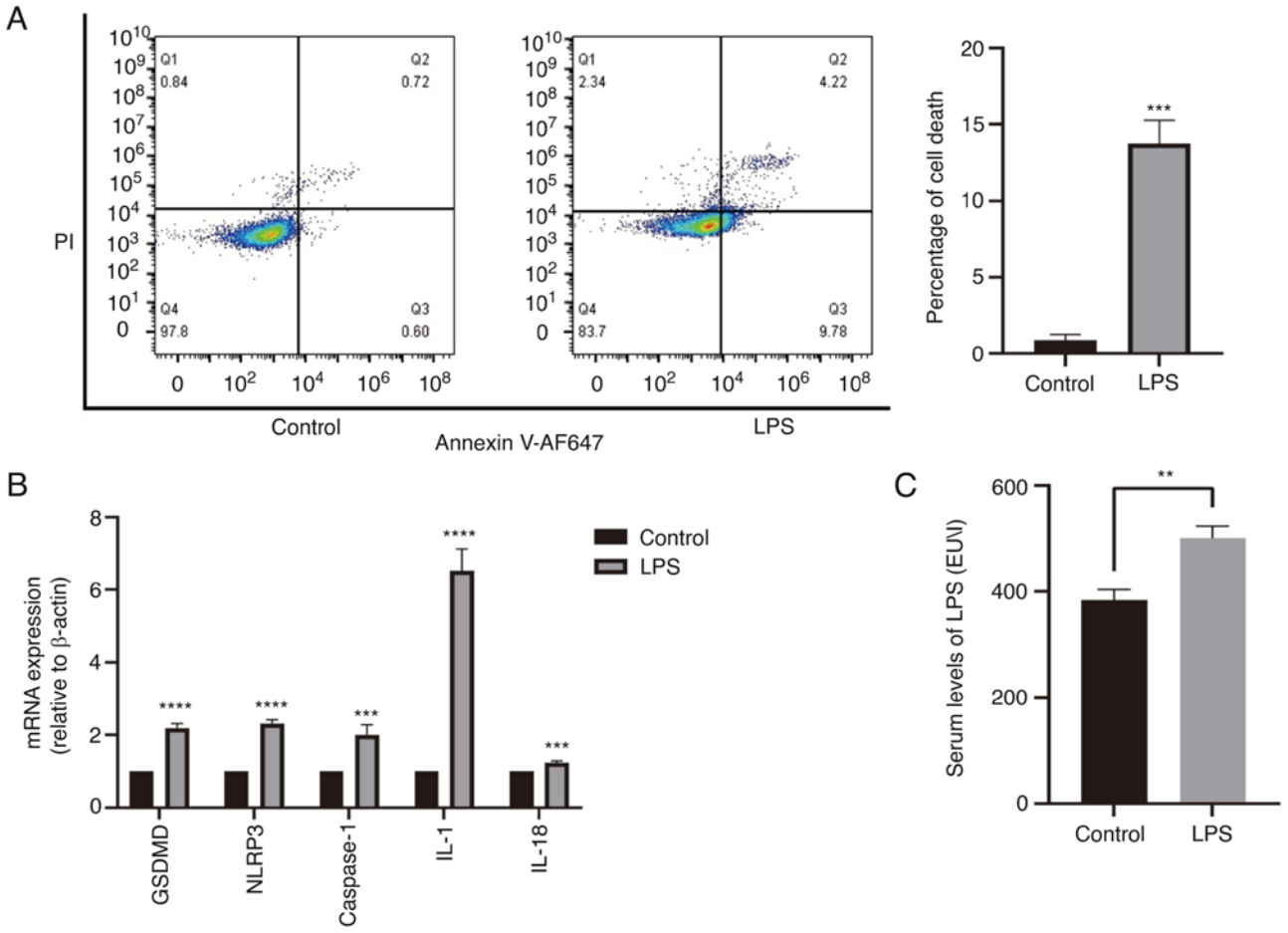

Figure 7. Flow cytometry and reverse transcription-quantitative PCR results. (A) Cell death incidence in the Control and LPS groups measured via flow cytometry. A significant increase in cell death rate is observed after 24 h of LPS treatment. (B) mRNA expression of pyroptotic pathway-related genes in RSC96 cells significantly increases following 24 h of LPS treatment. (C) Serum levels of LPS measured via ELISA. **P<0.01, ***P<0.001 and ****P<0.0001 vs. control. LPS, lipopolysaccharide; GSDMD, gasdermin D; NLRP3, NLR family pyrin domain containing 3; EU, EU, endotoxin unit.

nociceptors (57). The present ELISA results showed that the serum LPS level in the CCI model was increased compared with that in the sham group, so it was speculated that in the inflammatory environment, the pyroptosis of Schwann cells could inhibit the repair of neurons. Finally, it was found that LPS-induced RSC96 cells had higher expression levels of pyroptosis-related genes and higher rates of pyroptosis compared with those in the control group.

The present study aimed to classify patients with NP, discover NP-related genes, develop predictive models and establish a link between pyroptosis and patient outcomes. In conclusion, an NP-related pyroptosis gene signature was constructed based on four pyroptosis-related genes and it was determined that the expression of pyroptosis-related genes was upregulated during the beginning of the neuroinflammatory process in RSC96 cells.

There are certain shortcomings in the present study. The pyroptosis signature that was constructed in the present study would require external validation. However, to the best of our knowledge, there are few data on NP and there are no suitable datasets for external validation. In addition, the small number of rat samples was insufficient to measure the expression levels of these pyroptosis-related genes. Moreover, the present study did not investigate the LPS-induced secretion levels of neurotrophic factors in Schwann cells, such as nerve growth factor, brain-derived neurotrophic factor, neurotrophin (NT)-3, NT-4/5 and glial cell line-derived neurotrophic factor, therefore the relationship between pyroptosis and neurotrophic factor secretion cannot be fully explained. Furthermore, only RSC96 Schwann cells were used for validation and blood samples from clinical patients were not obtained. In the future, blood samples from clinical patients may be collected for further validation.

Acknowledgements

Not applicable.

Funding

This study was supported by The National Natural Science Foundation of China (grant no. 81874404).

Availability of data and materials

The datasets used and/or analysed during the current study are available from the corresponding author on reasonable request. Other datasets generated and/or analysed during the current

study are available in the GEO repository, https://www.ncbi.nlm.nih.gov/geo/query/acc.cgi?acc=GSE124272 and https://www.ncbi.nlm.nih.gov/geo/query/acc.cgi?acc=GSE150408.

Authors' contributions

XL, DZ and GZ contributed substantially to the experimental design, data analysis and experimental procedures. LG contributed to *in vitro* and *in vivo* experimental design. HS, BJ, ZC, SC and YZ contributed to immunohistochemistry and RT-qPCR. GZ is the corresponding author. XL and DZ confirm the authenticity of all the raw data. All authors have read and approved the final manuscript.

Ethics approval and consent to participate

All experimental protocols were approved by the Ethics Committee of Jinan University (Guangzhou, China; approval no. IACUC-20200115-04). All animal experiments were conducted following the guidelines established by the National Academy of Sciences, the National Institutes of Health and the Institute of Laboratory Animal Resources (US).

Patient consent for publication

Not applicable.

Competing interests

The authors declare that they have no competing interests.

References

1. Calmels P, Mick G, Perrouin-Verbe B and Ventura M; SOFMER (French Society for Physical Medicine and Rehabilitation): Neuropathic pain in spinal cord injury: Identification, classification, evaluation. Ann Phys Rehabil Med 52: 83-102, 2009.
2. Orhurhu MS, Chu R, Claus L, Roberts J, Salisu B, Urits I, Orhurhu E, Viswanath O, Kaye AD, Kaye AJ and Orhurhu V: Neuropathic Pain and sickle cell disease: A review of pharmacologic management. Curr Pain Headache Rep 24: 52, 2020.
3. Schestatsky P, Vidor L, Winckler PB, Araújo TG and Caumo W: Promising treatments for neuropathic pain. Arq Neuropsiquiatr 72: 881-888, 2014.
4. van Hecke O, Austin SK, Khan RA, Smith BH and Torrance N: Neuropathic pain in the general population: A systematic review of epidemiological studies. Pain 155: 654-662, 2014.
5. Gilron I, Baron R and Jensen T: Neuropathic pain: Principles of diagnosis and treatment. Mayo Clin Proc 90: 532-545, 2015.
6. McKenzie BA, Mamik MK, Saito LB, Boghozian R, Monaco MC, Major EO, Lu JQ, Branton WG and Power C: Caspase-1 inhibition prevents glial inflammasome activation and pyroptosis in models of multiple sclerosis. Proc Natl Acad Sci USA 115: E6065-E6074, 2018.
7. Zhang Y, Liu X, Bai X, Lin Y, Li Z, Fu J, Li M, Zhao T, Yang H, Xu R, *et al*: Melatonin prevents endothelial cell pyroptosis via regulation of long noncoding RNA MEG3/miR-223/NLRP3 axis. J Pineal Res 64 2018.
8. Sborgi L, Ruhl S, Mulvihill E, Pipercevic J, Heilig R, Stahlberg H, Farady CJ, Müller DJ, Broz P and Hiller S: GSDMD membrane pore formation constitutes the mechanism of pyroptotic cell death. EMBO J 35: 1766-1778, 2016.
9. Zhao B, Pan Y, Xu H and Song X: Hyperbaric oxygen attenuates neuropathic pain and reverses inflammatory signaling likely via the Kindlin-1/Wnt-10a signaling pathway in the chronic pain injury model in rats. J Headache Pain 18: 1, 2017.
10. Narita M, Yoshida T, Nakajima M, Narita M, Miyatake M, Takagi T, Yajima Y and Suzuki T: Direct evidence for spinal cord microglia in the development of a neuropathic pain-like state in mice. J Neurochem 97: 1337-1348, 2006.
11. Cheng YC, Chu LW, Chen JY, Hsieh SL, Chang YC, Dai ZK and Wu BN: Loganin attenuates high glucose-induced schwann cells pyroptosis by inhibiting ROS generation and NLRP3 Inflammasome Activation. Cells 9: 1948, 2020.
12. Morrens J, Van Den Broeck W and Kempermann G: Glial cells in adult neurogenesis. Glia 60: 159-174, 2012.
13. Kidd GJ, Ohno N and Trapp BD: Biology of Schwann cells. Handb Clin Neurol 115: 55-79, 2013.
14. Chen G, Zhang Z, Wei Z, Cheng Q, Li X, Li W, Duan S and Gu X: Lysosomal exocytosis in Schwann cells contributes to axon remyelination. Glia 60: 295-305, 2012.
15. Wei Z, Fei Y, Su W and Chen G: Emerging role of schwann cells in neuropathic pain: Receptors, glial mediators and myelination. Front Cell Neurosci 13: 116, 2019.
16. Wang Y, Dai G, Jiang L, Liao S and Xia J: Microarray analysis reveals an inflammatory transcriptomic signature in peripheral blood for sciatica. BMC Neurol 21: 50, 2021.
17. Wang Y, Dai G, Li L, Liu L, Jiang L, Li S, Liao S, Wang F, Du W and Li Y: Transcriptome signatures reveal candidate key genes in the whole blood of patients with lumbar disc prolapse. Exp Ther Med 18: 4591-4602, 2019.
18. Langfelder P and Horvath S: WGCNA: An R package for weighted correlation network analysis. BMC Bioinformatics 9: 559, 2008.
19. Ye Z, Zeng Z, Shen Y and Chen Z: Identification of hub genes in peripheral blood mononuclear cells for the diagnosis of hepatocellular carcinoma using a weighted gene co-expression network analysis. Exp Ther Med 20: 890-900, 2020.
20. Ye Y, Dai Q and Qi H: A novel defined pyroptosis-related gene signature for predicting the prognosis of ovarian cancer. Cell Death Discov 7: 71, 2021.
21. Xia X, Wang X, Cheng Z, Qin W, Lei L, Jiang J and Hu J: The role of pyroptosis in cancer: Pro-cancer or pro-'host'? Cell Death Dis 10: 650, 2019.
22. Kelley N, Jeltema D, Duan Y and He Y: The NLRP3 Inflammasome: An overview of mechanisms of activation and regulation. Int J Mol Sci 20: 3328, 2019.
23. Karki R and Kanneganti TD: Diverging inflammasome signals in tumorigenesis and potential targeting. Nat Rev Cancer 19: 197-214, 2019.
24. Ito K and Murphy D: Application of ggplot2 to pharmacometric graphics. CPT Pharmacometrics Syst Pharmacol 2: e79, 2013.
25. Zhang Z, Zeng X, Wu Y, Liu Y, Zhang X and Song Z: Cuproptosis-Related risk score predicts prognosis and characterizes the tumor microenvironment in hepatocellular carcinoma. Front Immunol 13: 925618, 2022.
26. Alba AC, Agoritsas T, Walsh M, Hanna S, Iorio A, Devereaux PJ, McGinn T and Guyatt G: Discrimination and calibration of clinical prediction models: Users' guides to the medical literature. JAMA 318: 1377-1384, 2017.
27. Zhang D, Sun J, Yang B, Ma S, Zhang C and Zhao G: Therapeutic effect of tetrapanax papyriferus and hederagenin on chronic neuropathic pain of chronic constriction injury of sciatic nerve rats based on KEGG pathway prediction and experimental verification. Evid Based Complement Alternat Med 2020: 2545806, 2020.
28. Yoon C, Wook YY, Sik NH, Ho KS and Mo CJ: Behavioral signs of ongoing pain and cold allodynia in a rat model of neuropathic pain. Pain 59: 369-376, 1994.
29. Livak KJ and Schmittgen TD: Analysis of relative gene expression data using real-time quantitative PCR and the 2(-Delta Delta C(T)) Method. Methods 25: 402-408, 2001.
30. Castro R, Taetzsch T, Vaughan SK, Godbe K, Chappell J, Settlage RE and Valdez G: Specific labeling of synaptic schwann cells reveals unique cellular and molecular features. Elife 9: e56935, 2020.
31. Zhang M, Qian C, Zheng ZG, Qian F, Wang Y, Thu PM, Zhang X, Zhou Y, Tu L, Liu Q, *et al*: Jujuboside A promotes Aβ clearance and ameliorates cognitive deficiency in Alzheimer's disease through activating Axl/HSP90/PPARγ pathway. Theranostics 8: 4262-4278, 2018.
32. Yu P, Zhang X, Liu N, Tang L, Peng C and Chen X: Pyroptosis: Mechanisms and diseases. Signal Transduct Target Ther 6: 128, 2021.
33. Ali MF, Dasari H, Van Keulen VP and Carmona EM: Canonical stimulation of the NLRP3 Inflammasome by fungal antigens links innate and adaptive B-Lymphocyte responses by modulating IL-1β and IgM production. Front Immunol 8: 1504, 2017.

34. Bhatnagar V, Gormley NJ, Luo L, Shen YL, Sridhara R, Subramaniam S, Shen G, Ma L, Shord S, Goldberg KB, *et al*: FDA approval summary: Daratumumab for treatment of multiple myeloma after one prior therapy. Oncologist 22: 1347-1353, 2017.
35. Chakraborty S, Kaushik DK, Gupta M and Basu A: Inflammasome signaling at the heart of central nervous system pathology. J Neurosci Res 88: 1615-1631, 2010.
36. Thakur V, Sadanandan J and Chattopadhyay M: High-Mobility group box 1 protein signaling in painful diabetic neuropathy. Int J Mol Sci 21: 881, 2020.
37. Liu CC, Huang ZX, Li X, Shen KF, Liu M, Ouyang HD, Zhang SB, Ruan YT, Zhang XL, Wu SL, *et al*: Upregulation of NLRP3 via STAT3-dependent histone acetylation contributes to painful neuropathy induced by bortezomib. Exp Neurol 302: 104-111, 2018.
38. Zhang A, Wang K, Ding L, Bao X, Wang X, Qiu X and Liu J: Bay11-7082 attenuates neuropathic pain via inhibition of nuclear factor-kappa B and nucleotide-binding domain-like receptor protein 3 inflammasome activation in dorsal root ganglions in a rat model of lumbar disc herniation. J Pain Res 10: 375-382, 2017.
39. Thawkar BS and Kaur G: Inhibitors of NF-κB and P2X7/NLRP3/Caspase 1 pathway in microglia: Novel therapeutic opportunities in neuroinflammation induced early-stage Alzheimer's disease. J Neuroimmunol 326: 62-74, 2019.
40. He Y, Hara H and Núñez G: Mechanism and regulation of NLRP3 inflammasome activation. Trends Biochem Sci 41: 1012-1021, 2016.
41. Mishra SR, Mahapatra KK, Behera BP, Patra S, Bhol CS, Panigrahi DP, Praharaj PP, Singh A, Patil S, Dhiman R and Bhutia SK: Mitochondrial dysfunction as a driver of NLRP3 inflammasome activation and its modulation through mitophagy for potential therapeutics. Int J Biochem Cell Biol 136: 106013, 2021.
42. Tschopp J and Schroder K: NLRP3 inflammasome activation: The convergence of multiple signalling pathways on ROS production? Nat Rev Immunol 10: 210-215, 2010.
43. Muñoz-Planillo R, Kuffa P, Martínez-Colón G, Smith BL, Rajendiran TM and Núñez G: K^+ efflux is the common trigger of NLRP3 inflammasome activation by bacterial toxins and particulate matter. Immunity 38: 1142-1153, 2013.
44. Zhou Y, Tong Z, Jiang S, Zheng W, Zhao J and Zhou X: The roles of endoplasmic reticulum in NLRP3 inflammasome activation. Cells 9: 1219, 2020.
45. Lee GS, Subramanian N, Kim AI, Aksentijevich I, Goldbach-Mansky R, Sacks DB, Germain RN, Kastner DL and Chae JJ: The calcium-sensing receptor regulates the NLRP3 inflammasome through Ca2+ and cAMP. Nature 492: 123-127, 2012.
46. Binshtok AM, Wang H, Zimmermann K, Amaya F, Vardeh D, Shi L, Brenner GJ, Ji RR, Bean BP, Woolf CJ and Samad TA: Nociceptors are interleukin-1beta sensors. J Neurosci 28: 14062-14073, 2008.
47. Woolf CJ and Ma Q: Nociceptors-noxious stimulus detectors. Neuron 55: 353-364, 2007.
48. Gan H, Zhang L, Chen H, Xiao H, Wang L, Zhai X, Jiang N, Liang P, Zheng S and Zhao J: The pivotal role of the NLRC4 inflammasome in neuroinflammation after intracerebral hemorrhage in rats. Exp Mol Med 53: 1807-1818, 2021.
49. Wang L, Negro R and Wu H: TRPM2, linking oxidative stress and Ca^{2+} permeation to NLRP3 inflammasome activation. Curr Opin Immunol 62: 131-135, 2020.
50. Zhao Y, Yang J, Shi J, Gong YN, Lu Q, Xu H, Liu L and Shao F: The NLRC4 inflammasome receptors for bacterial flagellin and type III secretion apparatus. Nature 477: 596-600, 2011.
51. Aachoui Y, Sagulenko V, Miao EA and Stacey KJ: Inflammasome-mediated pyroptotic and apoptotic cell death, and defense against infection. Curr Opin Microbiol 16: 319-326, 2013.
52. Liu X, Zhang Z, Ruan J, Pan Y, Magupalli VG, Wu H and Lieberman J: Inflammasome-activated gasdermin D causes pyroptosis by forming membrane pores. Nature 535: 153-158, 2016.
53. Conforti L, Gilley J and Coleman MP: Wallerian degeneration: An emerging axon death pathway linking injury and disease. Nat Rev Neurosci 15: 394-409, 2014.
54. Jessen KR, Mirsky R and Lloyd AC: Schwann cells: Development and role in nerve repair. Cold Spring Harb Perspect Biol 7: a020487, 2015.
55. Gomez-Sanchez JA, Carty L, Iruarrizaga-Lejarreta M, Palomo-Irigoyen M, Varela-Rey M, Griffith M, Hantke J, Macias-Camara N, Azkargorta M, Aurrekoetxea I, *et al*: Schwann cell autophagy, myelinophagy, initiates myelin clearance from injured nerves. J Cell Biol 210: 153-168, 2015.
56. Franchi S, Valsecchi AE, Borsani E, Procacci P, Ferrari D, Zaffa C, Sartori P, Rodella LF, Vescovi A, Maione S, *et al*: Intravenous neural stem cells abolish nociceptive hypersensitivity and trigger nerve regeneration in experimental neuropathy. Pain 153: 850-861, 2012.
57. De Logu F, Nassini R, Materazzi S, Carvalho Gonçalves M, Nosi D, Rossi Degl'Innocenti D, Marone IM, Ferreira J, Li Puma S, Benemei S, *et al*: Schwann cell TRPA1 mediates neuroinflammation that sustains macrophage-dependent neuropathic pain in mice. Nat Commun 8: 1887, 2017.